

# A cross-correlation-based estimate of the galaxy luminosity function

Marcel P. van Daalen<sup>1\*</sup> and Martin White<sup>1</sup>

<sup>1</sup>*Department of Astronomy, Theoretical Astrophysics Center, and Lawrence Berkeley National Laboratory,  
University of California, Berkeley, CA 94720, USA*

17 March 2017

## ABSTRACT

We extend existing methods for using cross-correlations to derive redshift distributions for photometric galaxies, without using photometric redshifts. The model presented in this paper simultaneously yields highly accurate and unbiased redshift distributions and, for the first time, redshift-dependent luminosity functions, using only clustering information and the apparent magnitudes of the galaxies as input. In contrast to many existing techniques for recovering unbiased redshift distributions, the output of our method is not degenerate with the galaxy bias  $b(z)$ , which is achieved by modelling the shape of the luminosity bias. We successfully apply our method to a mock galaxy survey and discuss the potential application of our model to real data.

**Key words:** galaxies: distances and redshifts – galaxies: luminosity function – cosmology: theory – cosmology: large-scale structure of Universe

## 1 INTRODUCTION

Current and planned large galaxy surveys are bringing in enormous amounts of photometric data. Spectroscopic follow-up for even a tenth of these sources is infeasible, and so many techniques have been developed to derive valuable redshift information indirectly for the vast majority of observed galaxies. Classically, estimating redshifts or redshift distributions has been performed using photometry in combination with a library of SEDs and/or spectroscopic sources to train the algorithms used, yielding a redshift (or redshift probability distribution) for each galaxy. However, these methods are not designed to yield unbiased redshift distributions, as they rely on the galaxies used in the training set to be representative of and similarly distributed to the overall population. Because of this, the accuracy of photometric redshifts (or photo- $z$ s) can depend strongly on e.g. the magnitude, redshift and type of a galaxy, and the filters used (e.g. Cunha et al. 2009, Bezanson et al. 2016).

An alternative way to obtain redshift distributions for photometric galaxies statistically is to examine how strongly they cluster with sources that have a known redshift. Even if these spectroscopic sources are a biased subset with a very different redshift distribution, they should still trace the same large-scale structure as the overall galaxy population. This means that it is statistically likely for galaxies to be at the same redshift as other sources they clus-

ter strongly with, i.e. if two galaxies are close on the sky then they are more likely to be close along the line of sight. Techniques exploiting clustering to obtain independent redshift information have been applied for a number of years now, to improve and/or characterize the errors of a photo- $z$  catalogue (e.g. Padmanabhan et al. 2007, Newman 2008, Erben et al. 2009, Kovač et al. 2010, Benjamin et al. 2010, Quadri & Williams 2010, Choi et al. 2016), reconstruct the density field (e.g. Jasche & Wandelt 2012, Malavasi et al. 2016, Cucciati et al. 2016) and to derive redshift distributions from clustering directly (e.g. Matthews & Newman 2010, Schulz 2010, McQuinn & White 2013, Ménard et al. 2013, Morrison et al. 2016). However, since this method is necessarily statistical we lose information on the properties of the galaxies in each redshift bin (although recently efforts have been made to introduce a dependence on colour, see Rahman et al. 2016). Additionally, the resulting distribution is often degenerate with the unknown redshift-dependent bias of the photometric sample,  $b(z)$ , which has to be removed in some way before the outcomes can be used (e.g. Schmidt et al. 2013).

Inspired by Sheth & Rossi (2010), we extend existing methods to find the number density of galaxies in not only bins of redshift,  $z$ , but also apparent magnitude,  $m$ . By simultaneously fitting for both distributions, luminosity functions in terms of absolute magnitude,  $M$ , can be extracted at different redshifts. This has great potential, as the luminosity function is a key observable of the galaxy population that offers powerful constraints on models of galaxy evolution.

\* E-mail: marcel@berkeley.edu

Extensive cosmological volumes are needed to measure it accurately, particularly at the bright end where galaxies are rare. Large imaging surveys offer this, but their redshift uncertainties lead to uncertainties in the absolute magnitude of the galaxies. Spectroscopic surveys, on the other hand, have small redshift uncertainties but can probe far fewer galaxies. By cross-correlating these two types of survey while taking the observed brightness of the galaxies into account, we can derive luminosity functions for large volumes with smaller redshift uncertainties than would be possible otherwise. This method also allows us to break degeneracies in a new way: by assuming a simple model for just the luminosity dependence of the galaxy bias, the resulting redshift distributions and luminosity functions are independent of  $b(z)$ , and no bias removal is necessary.

We present our method for simultaneously deriving redshift distributions and luminosity functions from clustering data in §2. As a test, we apply our model to a mock galaxy sample in §3. Finally, we summarize our results and discuss the possible limitations of our model when applied to real-world data in §4.

## 2 METHODOLOGY

The way in which we link the redshift distribution  $dN/dz$  to the clustering signal can be viewed as a combination of the methods employed by Schulz (2010) and Ménard et al. (2013), although we extend previous efforts by also estimating evolving luminosity functions for the photometric galaxies. Our approach is essentially to apply tomography to the luminosity function: the observed distribution of a sample of galaxies over apparent magnitude,  $n(m)$ , and the distributions of galaxies over redshift in bins of apparent magnitude,  $n_m(z)$ , can be viewed as projections of the underlying luminosity function as a function of redshift,  $\phi(M, z)$ , and therefore used to reconstruct it. An added advantage of fitting for the redshift distributions and luminosity functions simultaneously is that it allows one to make optimal use of the information available in the survey – for example, galaxies that appear bright are unlikely to be at high redshift, but traditional methods for deriving the redshift distributions do not account for this.

In what follows, subscripts “p” denote the photometric sample for which we aim to derive a distribution in magnitude and redshift, while subscripts “s” denote the spectroscopic sample (which has a known redshift distribution).

### 2.1 The cross-correlation signal

The number of sample galaxies in apparent magnitude bin  $m_\lambda$  and redshift bin  $z_i$  is given by:

$$N_p(m_\lambda, z_i) = \int_{z_{i,\min}}^{z_{i,\max}} \int_{m_{\lambda,\min}}^{m_{\lambda,\max}} \frac{dN_p}{dm dz}(m, z) dm dz, \quad (1)$$

where “ $i, \min$ ” and “ $i, \max$ ” denote the edges of bin  $i$ . The parameter we wish to extract from the data is the fraction of sample galaxies in apparent magnitude bin  $m_\lambda$  that reside in redshift bin  $z_i$ , given by:

$$f_N(m_\lambda, z_i) = \frac{N_p(m_\lambda, z_i)}{N_p(m_\lambda)}, \quad (2)$$

where  $N_p(m_\lambda)$  is the total number of galaxies in bin  $m_\lambda$ , given by:

$$N_p(m_\lambda) = \sum_i N_p(m_\lambda, z_i). \quad (3)$$

The  $N_p(m_\lambda)$  of the data are known *a priori*, however we do not enforce the  $N_p(m_\lambda)$  in our model – which we will refer to as  $\tilde{N}_p(m_\lambda)$  – to be identical to these. Rather, we interpret those in the data as being drawn from a Poisson distribution with means given by  $\tilde{N}_p(m_\lambda)$  (see §2.2).

As our signal we choose the integrated angular cross-correlation function of all photometric galaxies in apparent magnitude bin  $m_\lambda$  with the spectroscopic galaxies in redshift bin  $z_i$ ,  $\bar{w}_{ps}(m_\lambda, z_i)$ , given by:

$$\bar{w}_{ps}(m_\lambda, z_i) = \int_{\theta_{\min}}^{\theta_{\max}} w_{ps}(m_\lambda, z_i, \theta) W(\theta) d\theta, \quad (4)$$

where  $W(\theta)$  is a weight function. We follow Ménard et al. (2013) in choosing  $W(\theta) = \theta^{-1}$ , and for the purposes of illustration choose  $\theta_{\min} = 0.02$  and  $\theta_{\max} = 10$  degrees.

We will refer to our model for  $\bar{w}_{ps}(m_\lambda, z_i)$  as  $\tilde{w}_{ps}(m_\lambda, z_i)$ . This quantity is related to the integrated angular correlation function between spectroscopic galaxies in redshift bin  $z_i$  and those in redshift bin  $z_j$ ,  $\bar{w}_{ss}(z_i, z_j)$ , through:

$$\tilde{w}_{ps}(m_\lambda, z_i) = \sum_j f_N(m_\lambda, z_j) \frac{\bar{b}_p(m_\lambda, z_j)}{\bar{b}_s(z_j)} \bar{w}_{ss}(z_i, z_j), \quad (5)$$

where  $\bar{b}$  is the (linear) galaxy bias averaged over all scales  $\theta$  between  $\theta_{\min}$  and  $\theta_{\max}$ . Here we have used that the two samples trace the same underlying density field.

Both  $\bar{w}_{ps}$  and  $\bar{w}_{ss}$  can be directly calculated from the data (e.g. through pair counting), but the galaxy biases are *a priori* unknown. However, it is not unreasonable to assume that  $\bar{b}_p$  and  $\bar{b}_s$  evolve similarly with redshift at fixed luminosity, i.e.  $\bar{b}_p(m, z) = \bar{b}_{p,0} b_L(m, z) f(z)$  and  $\bar{b}_s(z) = \bar{b}_{s,0} f(z)$ .<sup>1</sup> Here  $b_L$  is some function of luminosity – assumed to be known, either independently or determined from the spectroscopic sample – with no residual dependence on  $m$  or  $z$ .

Next, we recognize that the redshift evolution  $f(z)$  of the biases cancels out when taking the ratio, and absorb all constants in a new term. Then, in the limit of infinitely accurate measurements of  $\bar{w}_{ps}(m_\lambda, z_i)$  and  $\bar{w}_{ss}(z_i, z_j)$  we can derive  $f_N$  simply by solving (for all  $z_i$ ):

$$\tilde{w}_{ps}(m_\lambda, z_i) = \sum_j f'_N(m_\lambda, z_j) \bar{w}_{ss}(z_i, z_j), \quad (6)$$

where  $f'_N(m_\lambda, z_j) = K b_L(m_\lambda, z_j) N_p(m_\lambda, z_j) / N_p(m_\lambda)$  with  $K$  an unknown constant and a parameter of the model. This set of equations can be written as  $\tilde{\mathbf{w}}_{ps}(m_\lambda) = \mathbf{X} \mathbf{f}'_N(m_\lambda)$ , with  $\tilde{\mathbf{w}}_{ps}(m_\lambda)$  and  $\mathbf{f}'_N(m_\lambda)$  vectors of length  $n_z$  and  $\mathbf{X}$  a matrix of size  $n_z \times n_z$ , where  $n_z$  is the number of redshift bins. Hence,  $X_{ij} = \bar{w}_{ss}(z_i, z_j)$ . Note that we do not assume the often-used Limber approximation, but allow for non-zero cross-correlations between redshift bins. In §3.2, we show how our results are affected if these cross-correlations are assumed to be zero.

<sup>1</sup> Alternatively,  $\bar{b}_s(z)$  could be estimated from the data (propagating the observational uncertainties) and  $\bar{b}_p(m, z)$  (or the ratio) could be modelled (e.g. as a polynomial in redshift).

For the purposes of illustration, we choose the following simple form for the luminosity bias:

$$b_L(m, z) = 1 + \frac{L(m, z)}{L'}, \quad (7)$$

where  $L(m, z)$  is the luminosity of a galaxy of apparent magnitude  $m$  at redshift  $z$ . We set  $L'$  to be the luminosity of a galaxy with absolute magnitude  $M' = -23.3$ . Note that the normalization of the luminosity bias is indirectly controlled by the model parameter  $K$ .

At this point, we could solve the equations given by  $\tilde{\mathbf{w}}_{\text{ps}}(m_\lambda) = \mathbf{X} \mathbf{f}'_{\text{N}}(m_\lambda)$  for every  $m_\lambda$  independently to find the corresponding galaxy redshift distributions. However, this disregards the information inherent in the apparent magnitudes of the galaxies. Since the clustering measurements have uncertainty (and since there may be degenerate solutions), this will likely lead to, for example, at least some galaxies with a very bright apparent magnitude being placed at high redshift – corresponding to an unphysically high luminosity. Luminosity functions fitted to these results will therefore be extremely biased and unrealistic.

By fitting to the redshift distribution and the luminosity functions of the sample galaxies simultaneously, we avoid such biased outcomes. This requires us to explicitly model  $N_p(m_\lambda, z_i)$ .

For conciseness, we will use a subscript notation for binned quantities, i.e.  $N_{p, \lambda i} \equiv N_p(m_\lambda, z_i)$ , where Greek subscripts always refer to the apparent magnitude bin and Latin subscripts to the redshift bin. Since we fit our model to all bins simultaneously, it is useful to think in terms of superindices  $(\lambda i) = n_\lambda \lambda + i$ . We will omit the parentheses where it does not lead to confusion.

## 2.2 A model for $N_p(m, z)$

$N_{p, \lambda i}$  is shaped by the luminosity function, which determines the number density of galaxies at apparent magnitude  $m_\lambda$  and redshift  $z_i$ , and the survey volume at redshift  $z_i$ . Figure 1 illustrates how these two quantities combine to form the redshift distribution of galaxies at fixed apparent magnitude. In this example we assume that both the luminosity function and the total number density of galaxies are constant with redshift. We consider galaxies in a fixed apparent magnitude bin, although the principle applies to any magnitude-limited survey. As the survey volume grows with redshift, the number of galaxies observed per unit redshift increases. However, galaxies with a fixed apparent magnitude correspond to increasingly more-luminous and more-rare galaxies, and so the number density decreases with redshift, first as a power law and then exponentially. The combined result of these two competing effects is a galaxy redshift distribution  $dN/dz \propto \Delta\Phi\Delta V$  that increases as a power law before decreasing exponentially.<sup>2</sup>

Assuming a cosmology fixes the evolution of the survey volume. The shape of the luminosity function at each  $z$  then fixes the redshift distribution. Conversely, knowing both the

cosmology and the redshift distribution at several fixed apparent magnitudes gives us information on the shape of the luminosity function through cosmic time.

The comoving distance (for a flat  $\Lambda$ CDM universe) is given by:

$$d_c(z) = \int_0^z \frac{c}{H_0 \sqrt{\Omega_{m,0}(1+z')^3 + \Omega_{\Lambda,0}}} dz', \quad (8)$$

and hence the volume in redshift bin  $i$  by:

$$\begin{aligned} V_i &= \int_A \int_{d_{i,\min}}^{d_{i,\max}} d_c(z)^2 dd(z) dA \\ &= f(A) 4\pi \int_{z_{i,\min}}^{z_{i,\max}} \frac{d_c(z)^2 c}{H_0 \sqrt{\Omega_{m,0}(1+z)^3 + \Omega_{\Lambda,0}}} dz, \end{aligned} \quad (9)$$

where  $A$  is the area on the sky the survey covers and  $f(A)$  is the fraction of the sky (in units of steradians) covered, and where the limits of integration  $z_{i,\min}$  and  $z_{i,\max}$  are the minimum and maximum redshift values respectively of redshift bin  $i$ .

For the purposes of illustration, we will assume the luminosity function is described well by a single Schechter function. We further assume that its parameters  $\alpha$  (the low-luminosity power-law slope) and  $M_*$  (the turn-over absolute magnitude) evolve linearly with redshift, that is  $\alpha = \alpha_0 + \alpha_e z$  and  $M_* = M_{*0} + M_{*e} z$ . The normalization of the luminosity function is allowed to evolve with redshift as well; specifically, we model it as the exponential of a 5th-order polynomial, as follows:

$$\phi_*(z) = \exp \left( \sum_{j=0}^5 \zeta_j \left[ \frac{2z}{z_{\max}} - 1 \right]^j \right), \quad (10)$$

with  $z_{\max}$  the maximum redshift considered and six free parameters  $\zeta_j$ . Our luminosity function thus has 10 free parameters in total. We note that the luminosity function can be straightforwardly generalized to include e.g. additional Schechter terms or a more (or less) sophisticated redshift evolution.

To avoid divergence (and because there exists a minimum luminosity to what is considered a galaxy), we define a limiting galaxy absolute magnitude  $M_{\text{lim}}$ . In this study we set  $M_{\text{lim}} = -16$ , but we note that any sufficiently dim value of  $M_{\text{lim}}$  does not influence the outcome of the model. The (integrated) number density of galaxies in apparent magnitude bin  $m_\lambda$  and redshift bin  $z_i$  is then:

$$\begin{aligned} \Phi_{\lambda i} &= \frac{2}{5} \ln(10) \int_{z_{i,\min}}^{z_{i,\max}} \phi_*(z) \times \\ &\int_{M_1}^{M_2} \frac{10^{\frac{2}{5}(M_*(z) - M(m, z))(\alpha(z) + 1)} e^{-10^{\frac{2}{5}(M_*(z) - M(m, z))}}}{\Gamma(\alpha(z) + 1, 10^{\frac{2}{5}(M_*(z) - M_{\text{lim}})})} dM dz, \end{aligned} \quad (11)$$

where  $M(m, z)$  is the absolute magnitude corresponding to a galaxy with apparent magnitude  $m$  at redshift  $z$ .<sup>3</sup> Here we have defined the number density such that

<sup>2</sup> In the case of an evolving luminosity function, the integral over the sky and the luminosity function do not separate out as neatly as in this example, but the end result is similar. We do not make the assumption of a redshift-independent luminosity function beyond this example.

<sup>3</sup> In reality, the conversion from apparent to absolute magnitude would involve calculating a K-correction. Here we make the simplified assumption of a flat galaxy spectrum, in which case the K-correction is zero and  $M(m, z) = m + 5 [1 - \log_{10}(d_L(z))]$ , with  $d_L(z)$  the luminosity distance. We also ignore higher-order effects like lensing magnification.

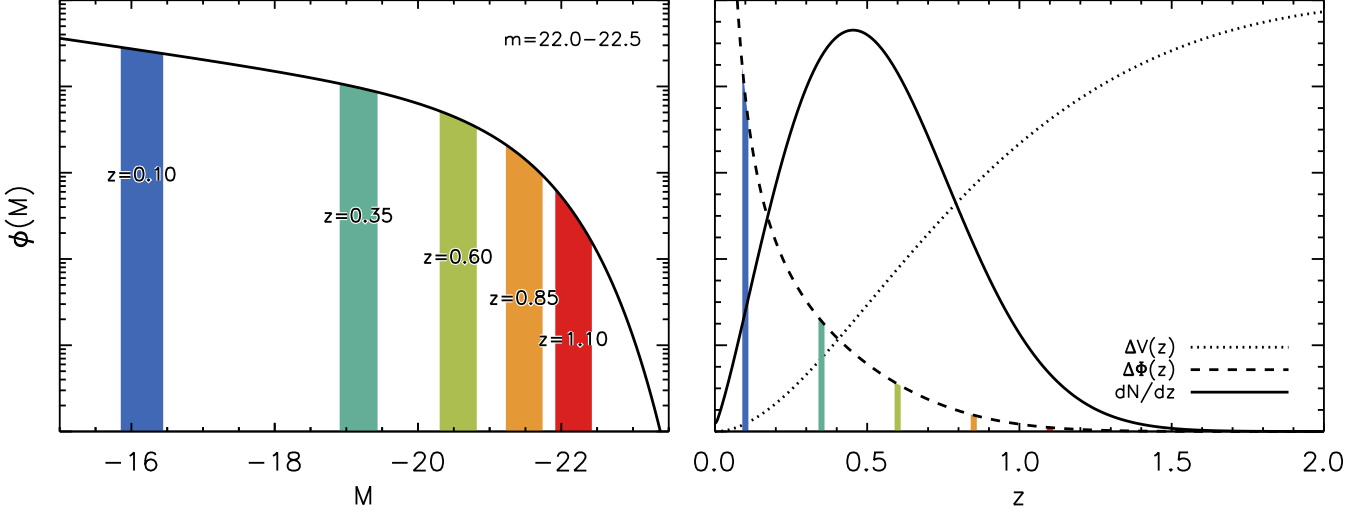


**Figure 1.** The survey volume and the luminosity function combine to form the redshift distribution  $dN/dz$ . Shown here is an example for galaxies in an apparent magnitude bin  $m = [22, 22.5]$ . *Left:* A Schechter (1976) luminosity function, with arbitrary normalization, as a function of absolute magnitude  $M$ . Here  $(\alpha, M_*) = (-1.3, -21.1)$ . Coloured regions show the absolute magnitudes corresponding to  $m = [22, 22.5]$  at redshifts  $z = 0.1, 0.35, 0.6, 0.85$  and  $1.1$  as indicated in the figure. In this example we assume the luminosity function is independent of redshift. *Right:* Shown together here are the comoving volume added by each redshift slice,  $\Delta V(z)$ , the Schechter function shown on the left integrated over the relevant range in  $M$ ,  $\Delta\Phi(M)$ , and the redshift distribution resulting from their product,  $dN/dz = \Delta\Phi\Delta V$ . The integral over one of the highlighted regions in the left-hand panel corresponds to the highlighted height of  $\Delta\Phi(M)$  in the right-hand panel.

$\int_{-\infty}^{M_{\text{lim}}} \frac{d\Phi_{\lambda i}}{dM_{\lambda i}} dM \equiv \int_{-\infty}^{M_{\text{lim}}} \phi_i(M) dM = \int \phi_*(z) dz_i$ . The limits of integration for  $M$  in equation (11) are determined by the edges of the bins  $m_{\lambda}$  and  $z_i$ , but the former are bounded above by  $M_{\text{lim}}$ . That is,  $M_1 = \min\{M(m_{\lambda, \text{min}}; z), M_{\text{lim}}\}$  and  $M_2 = \min\{M(m_{\lambda, \text{max}}; z), M_{\text{lim}}\}$ .

To account for evolution within each redshift bin, we simultaneously integrate the volume and the luminosity function. The Poisson mean in apparent magnitude bin  $m_{\lambda}$  and redshift bin  $z_i$  is then given by:<sup>4</sup>

$$\begin{aligned} \tilde{N}_{p, \lambda i} &= \int_{z_{i, \text{min}}}^{z_{i, \text{max}}} \int_{m_1}^{m_2} \frac{d\phi_i(M)}{dz_i} \frac{dV}{dz} dm dz \\ &= \frac{2}{5} \ln(10) B \int_{z_{i, \text{min}}}^{z_{i, \text{max}}} \frac{d_c(z)^2 \phi_*(z)}{\sqrt{\Omega_{m,0}(1+z)^3 + \Omega_{\Lambda,0}}} \times \\ &\quad \int_{m_1}^{m_2} \frac{10^{\frac{2}{5}(M_*(z) - M(m, z))(\alpha(z)+1)} e^{-10^{\frac{2}{5}(M_*(z) - M(m, z))}}}{\Gamma(\alpha(z) + 1, 10^{\frac{2}{5}(M_*(z) - M_{\text{lim}})})} dm dz, \end{aligned} \quad (12)$$

where some of the constants have been absorbed into the constant  $B$ ; specifically,  $B = 4\pi f(A) c/H_0$ . We have switched the integral over  $M$  to an integral over  $m$ , but similar to before,  $m_1 = \min\{m_{\lambda, \text{min}}; m(M_{\text{lim}}, z)\}$  and  $m_2 = \min\{m_{\lambda, \text{max}}; m(M_{\text{lim}}, z)\}$ . The integral over apparent magnitude has an analytical solution, and so we can reduce the above expression for the Poisson mean to an in-

tegral over only the redshift bin  $z_i$ :

$$\begin{aligned} \tilde{N}_{p, \lambda i} &= B \int_{z_{i, \text{min}}}^{z_{i, \text{max}}} \frac{d_c(z)^2 \phi_*(z)}{\sqrt{\Omega_{m,0}(1+z)^3 + \Omega_{\Lambda,0}}} \times \\ &\quad \left[ \Gamma(\alpha(z) + 1, 10^{\frac{2}{5}(M_*(z) - M_{\text{lim}})}) \right]^{-1} \times \\ &\quad \left[ \Gamma(\alpha(z) + 1, 10^{\frac{2}{5}(M_*(z) - M(m_2, z))}) - \right. \\ &\quad \left. \Gamma(\alpha(z) + 1, 10^{\frac{2}{5}(M_*(z) - M(m_1, z))}) \right] dz. \end{aligned} \quad (13)$$

The total number of model galaxies in apparent magnitude bin  $m_{\lambda}$  at any redshift is then:

$$\begin{aligned} \tilde{N}_{p, \lambda} &= \sum_i \tilde{N}_{p, \lambda i} \\ &= B \int_{z_{\text{min}}}^{z_{\text{max}}} \frac{d_c(z)^2 \phi_*(z)}{\sqrt{\Omega_{m,0}(1+z)^3 + \Omega_{\Lambda,0}}} \times \\ &\quad \left[ \Gamma(\alpha(z) + 1, 10^{\frac{2}{5}(M_*(z) - M_{\text{lim}})}) \right]^{-1} \times \\ &\quad \left[ \Gamma(\alpha(z) + 1, 10^{\frac{2}{5}(M_*(z) - M(m_{\text{max}}, z))}) - \right. \\ &\quad \left. \Gamma(\alpha(z) + 1, 10^{\frac{2}{5}(M_*(z) - M(m_{\text{min}}, z))}) \right] dz. \end{aligned} \quad (14)$$

Here  $z_{\text{min}}$  and  $z_{\text{max}}$  are the limits of the redshift range probed by the spectroscopic sample, and  $m_{\text{min}}$  and  $m_{\text{max}}$  are the limiting apparent magnitudes of the survey, taking into account  $M_{\text{lim}}$ . These model estimates of the mean can be directly compared to the  $N_{p, \lambda}$  of the data as a measure of our model's accuracy for a given set of parameters.

### 2.3 Fitting the model

Using 11 free parameters in total (1 parameter for the bias ratio, 6 for the normalization of the luminosity function and

<sup>4</sup> We note here that we ignore the modulation of observed galaxy number densities due to lensing magnification, which causes a magnification bias.

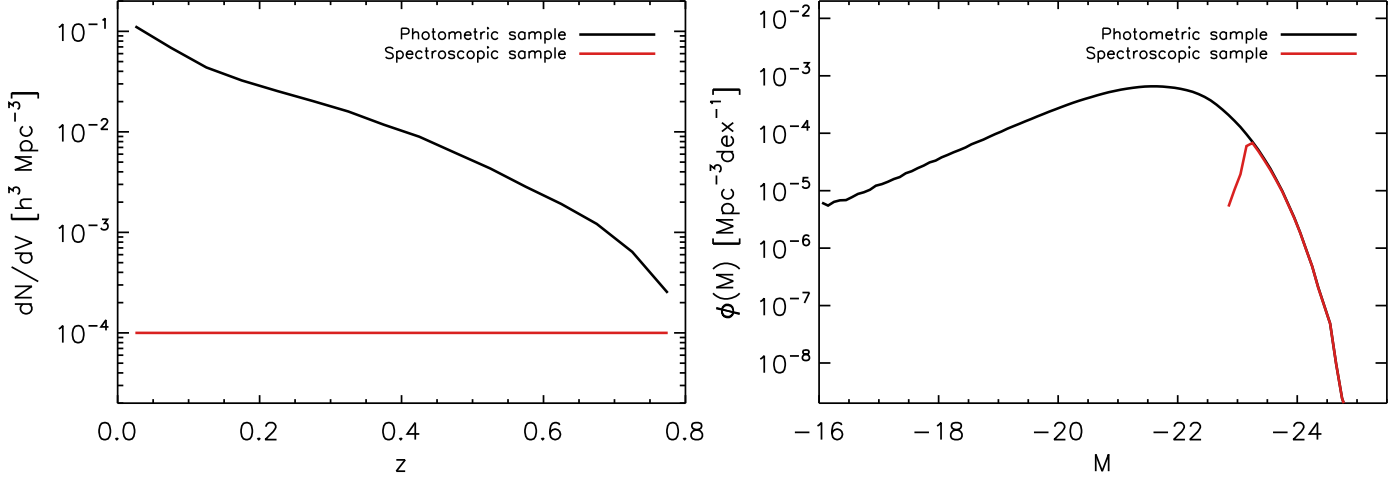


**Figure 2.** The distribution over cosmic (comoving) volume and absolute magnitude for our photometric (in black) and spectroscopic (in red) mock galaxy samples. By construction, the spectroscopic sample has a spatial density of  $10^{-4} (\text{Mpc}/h)^{-3}$  over the entire redshift range and contains only the most luminous (star-forming) galaxies. Even though this is a (realistically) biased subset of the total galaxy population, this sample can still be used to derive accurate redshift distributions and luminosity functions for the photometric galaxies, as they change the same large-scale structure and the clustering bias of the samples does not need to be known in our model.

4 for its shape parameters), our model predicts a distribution of galaxies in both absolute magnitude and redshift, and – using the observed integrated autocorrelation of the spectroscopic sample  $\tilde{w}_{ss,ij}$  – the corresponding cross-correlation signal  $\tilde{w}_{ps,\lambda i}$ . The best-fit set of parameters is determined by comparing the model outcomes  $\tilde{w}_{ps,\lambda i}$  and  $\tilde{N}_{p,\lambda}$  to their observed counterparts. We fit for these two quantities simultaneously by minimizing:

$$\chi^2 = (\tilde{\mathbf{w}}_{ps} - \tilde{\mathbf{w}}_{ps})^T C^{-1} (\tilde{\mathbf{w}}_{ps} - \tilde{\mathbf{w}}_{ps}) + R \sum_{\lambda} \frac{(N_{p,\lambda} - \tilde{N}_{p,\lambda})^2}{\tilde{\sigma}_{\lambda}^2}, \quad (15)$$

where  $C$  is a joint covariance matrix combining different sources of uncertainty in both the data and the model (see Appendix A),  $R$  is a constant determining the relative weight of the two observables, and  $\tilde{\sigma}_{\lambda}^2$  is the variance of  $\tilde{N}_{p,\lambda}$ . Since  $\tilde{N}_{p,\lambda}$  is a Poisson mean,  $\tilde{\sigma}_{\lambda}^2 = \tilde{N}_{p,\lambda}$ . The ideal value of  $R$  is unknown, but it should be set such that  $\tilde{N}_{p,\lambda}$  is not fit at the expense of  $\tilde{w}_{ps,\lambda i}$ , but rather used to break degeneracies in the clustering.<sup>5</sup> In what follows, we set  $R = 0.01$ . Very similar results are obtained if we vary  $R$  within a factor of 10.

### 3 TESTING THE MODEL

#### 3.1 Mock catalogues

To test our model, we extract a mock galaxy survey from one of the Planck Millennium all-sky lightcones released with Henriques et al. (2015).<sup>6</sup> In order to measure our model's performance, we have to know the luminosity function of

the data. We therefore reassign the absolute magnitude of each galaxy so that it is consistent with an input luminosity function. This is done in redshift bins 0.01 wide, and in such a way that the rank ordering of galaxies in brightness in each redshift bin is preserved (i.e. the  $N$  brightest galaxies at each redshift before reassignment are still the  $N$  brightest galaxies after reassignment, for every  $N$ ). We choose the shape parameters of our Schechter function to be  $\{\alpha_0, \alpha_e z, M_{*0}, M_{*e} z\} = \{-1.01, -0.15, -21.5, -0.8\}$  (see §2.2). These parameters were chosen to closely resemble the intrinsic luminosity function of the galaxies in the lightcone. We do not change the locations or number densities as a function of redshift of the galaxies, hence the normalization of the luminosity function and the clustering bias of the galaxies is still determined by the processes that formed them. We then make cuts in apparent magnitude and redshift, only keeping galaxies for which  $m \leq 21$  and  $z \leq 0.8$ . Next, we arbitrarily select the region with right ascension within  $[100, 200]$  degrees and declination within  $[10, 50]$  degrees, equivalent to  $3394 \text{ deg}^2$  or about 8% of the sky.

The galaxies that are left comprise our photometric galaxy sample. From it, we select a spectroscopic sample by selecting the  $N$  brightest galaxies in each redshift bin with stellar masses  $M_* \geq 10^{10} h^{-1} M_{\odot}$  and star formation rates  $\dot{M}_* \geq 1 h^{-1} M_{\odot}/\text{yr}$ , where  $N$  is chosen such that the number density of spectroscopic galaxies is at most  $10^{-4} (\text{Mpc}/h)^{-3}$  at every redshift. For the photometric sample we retain only the position on the sky and apparent magnitude. Finally, we take  $n_z = 16$  redshift bins,  $\Delta z = 0.05$  wide, in the range  $z = [0, 0.8]$ , and  $n_m = 16$  apparent magnitude bins,  $\Delta m = 0.5$  wide, in the range  $m = [13, 21]$ , and calculate the relevant (cross-)correlation functions and covariance matrices. In total, our photometric sample contains 14,280,584 galaxies that fall in these ranges, and our spectroscopic sample contains 250,372 sources.

We note that the spectroscopic sample is a (realisti-

<sup>5</sup> Note that the ideal weight should also depend on the number of redshift bins.

<sup>6</sup> Specifically, we use the catalogues “cones.AllSky\_M05\_001” and “MRscPlanck1” from the “Henriques2015a” part of the Millennium public database.

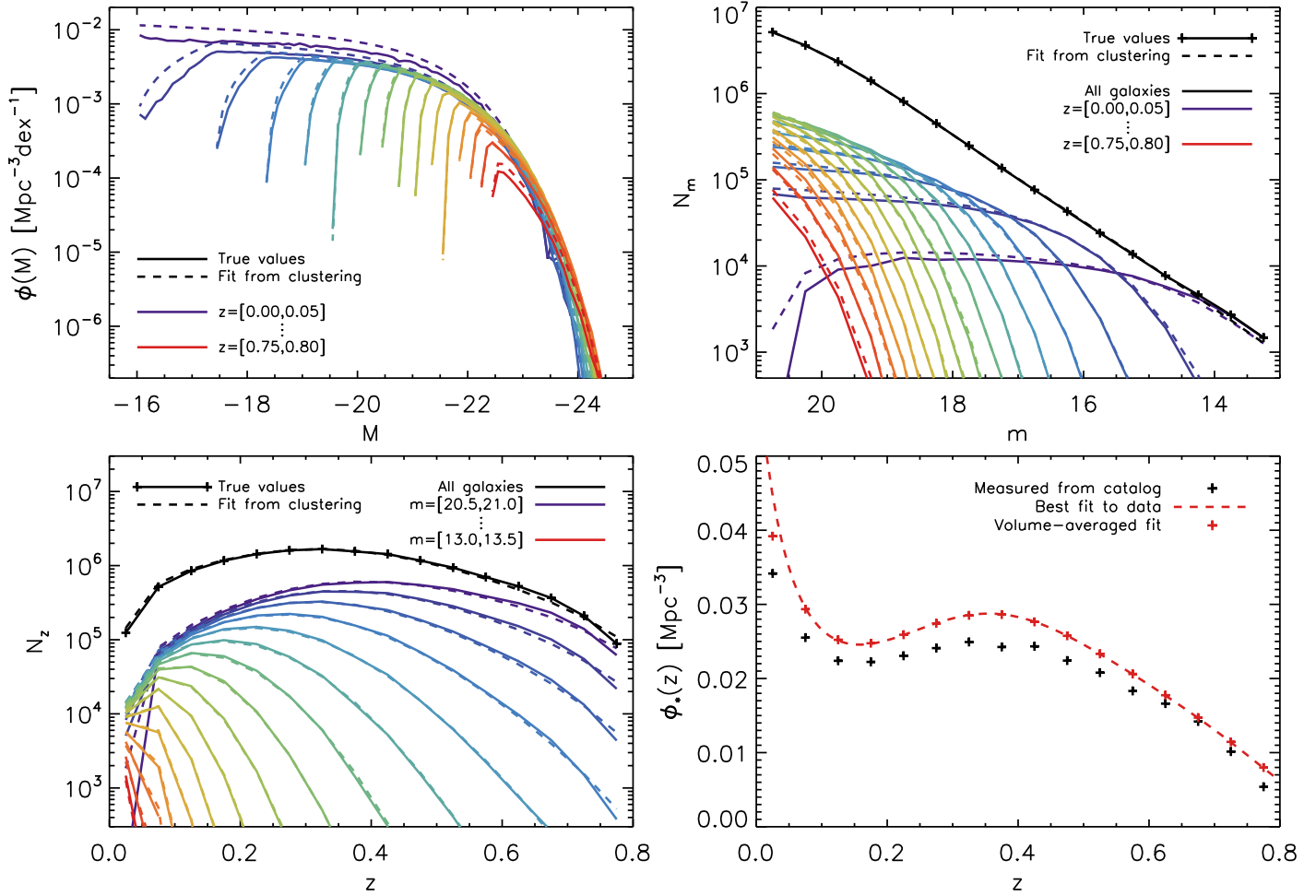


**Figure 3.** The results for our fiducial model, minimized using equation (15). The model is constrained by two sets of data, one being the cross-correlation signal between photometric and spectroscopic galaxies (in bins of the apparent magnitude of the former and the redshift of the latter), the other being the total number of photometric galaxies in each bin of apparent magnitude. *Top left:* The number of galaxies in different bins of redshift as a function of absolute magnitude. Solid lines show the data, dashed lines show the outcome of the model. Note that the power-law part of the Schechter function is only probed by low-redshift galaxies. Overall the luminosity function of the data is reproduced very well. The slight mismatch in the dropoff at the dim end (especially for second redshift bin) is due in part to how magnitudes were reassigned in the catalogues. For the first redshift bin, where the deviation between the derived and true galaxy densities is largest, the vertical offset is consistent with cosmic variance for the sky area we are using here. *Top right:* The number of galaxies in different bins of redshift as a function of apparent magnitude. The total over all redshifts, shown by the black line, is one of the constraints of the model. *Bottom left:* The number of galaxies in different bins of apparent magnitude as a function of redshift. Black lines show the total over all apparent magnitudes. *Bottom right:* The normalization of the Schechter luminosity function as a function of redshift. The normalizations as inferred from the mock catalogue are shown as black crosses while what the best-fit model prefers is shown as a red dashed line. Red crosses show the result of volume-averaging the best fit over each redshift bin.

cally) biased subset of the galaxy population. As we show in Figure 2, the spectroscopic galaxies have a radically different redshift distribution and only probe the most luminous end of the total luminosity function. However, since both samples still trace the same large-scale distribution, and since the bias ratio of the two samples is a free parameter in the model, this is not an issue in our approach. Indeed, Scottez et al. (2016) recently showed that for the similar methodology of Ménard et al. (2013), accurate redshift distributions can be obtained for galaxies fainter than those of the spectroscopic sample. Our own results in the following section confirm this.

### 3.2 Results

Using only the clustering amplitude of the spectroscopic sources and the total distribution of photometric galaxies over apparent magnitude, our model is able to reproduce the input luminosity function of the mock catalogue to very high accuracy. The results for our fiducial model are shown in Figure 3.

In the top-left panel, we show the luminosity functions as a function of absolute magnitude in for each redshift bin. Solid lines show the luminosity function as measured directly from the mock catalogue with full redshift information, thereby including realisation noise (which plays a significant role in the first two redshift bins). At low redshift,

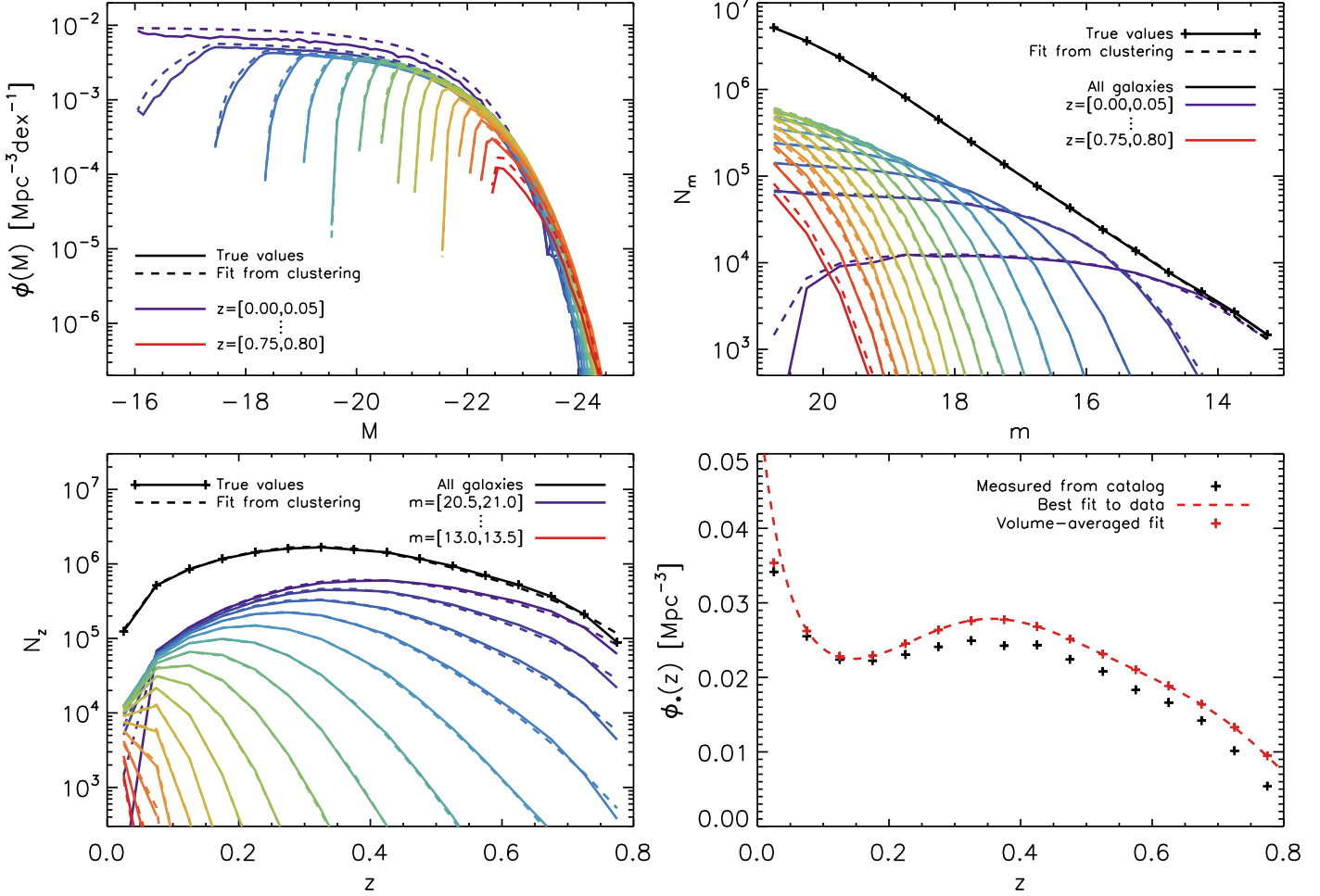


**Figure 4.** As Figure 3, but now  $\alpha_0$ , the power-law slope of the luminosity function at  $z = 0$ , was assumed known and held fixed to the input value in the fitting. As expected, this marginally improves the fit at low redshift.

the model tends to underestimate the number of dim galaxies, although we note that, at least for the first redshift bin, the mismatch is consistent with the uncertainty due to cosmic variance for our chosen sky area. We also note that the mismatch for the drop-off at the dim end – which is especially noticeable for the second redshift bin – is in part an artefact of how absolute magnitudes were reassigned to the mock galaxies (see §3.1). Even with these caveats, in most regimes the luminosity function of the mock galaxies are very accurately reproduced by the best-fit galaxy distribution, including the bright and dim end dropoffs. The latter is due to the cut-off apparent magnitude shifting to brighter galaxies within each redshift bin, and therefore only captured when the model luminosity function and volume are integrated together (see (12)).

We show the distribution over apparent magnitude for each redshift bin in the top-right panel. The total distribution is shown in black, and is used as a constraint in the model to break the clustering degeneracies (see equation (15)). The model again tends to both slightly underestimate the number of bright galaxies and overestimate the number of dim galaxies in the lowest redshift bin, where the clustering signal has a relatively large uncertainty. Overall, though, the model does very well in reproducing the true

distribution of galaxies in apparent magnitude, at any redshift.

The bottom-left panel of Figure 3 shows the redshift distributions in each apparent magnitude bin, as well as the total. Note that we are showing the absolute number of galaxies assigned to each redshift bin. The clustering model does an excellent job at reproducing these, even for the bright galaxies with relatively low number densities. As before, the fit is particularly accurate at intermediate redshifts (for all apparent magnitudes), where most of the constraining power is.

Finally, in the bottom-right panel, we show the normalization of the luminosity function as a function of redshift. Black crosses show the effective normalization of the mock galaxies in the survey area in each redshift bin. The dashed red line shows the fit (see equation (10)) that best reproduced the clustering data, with red crosses showing its volume-averaged values in each redshift bin to allow for a more direct comparison to the input data. The fit captures the shape of the input data, even if it tends to overestimate the normalization. However, due to the degeneracies between different Schechter parameters, particularly at high redshift (i.e. beyond the knee of the luminosity function), a mismatch in the value of the normalization parameter does



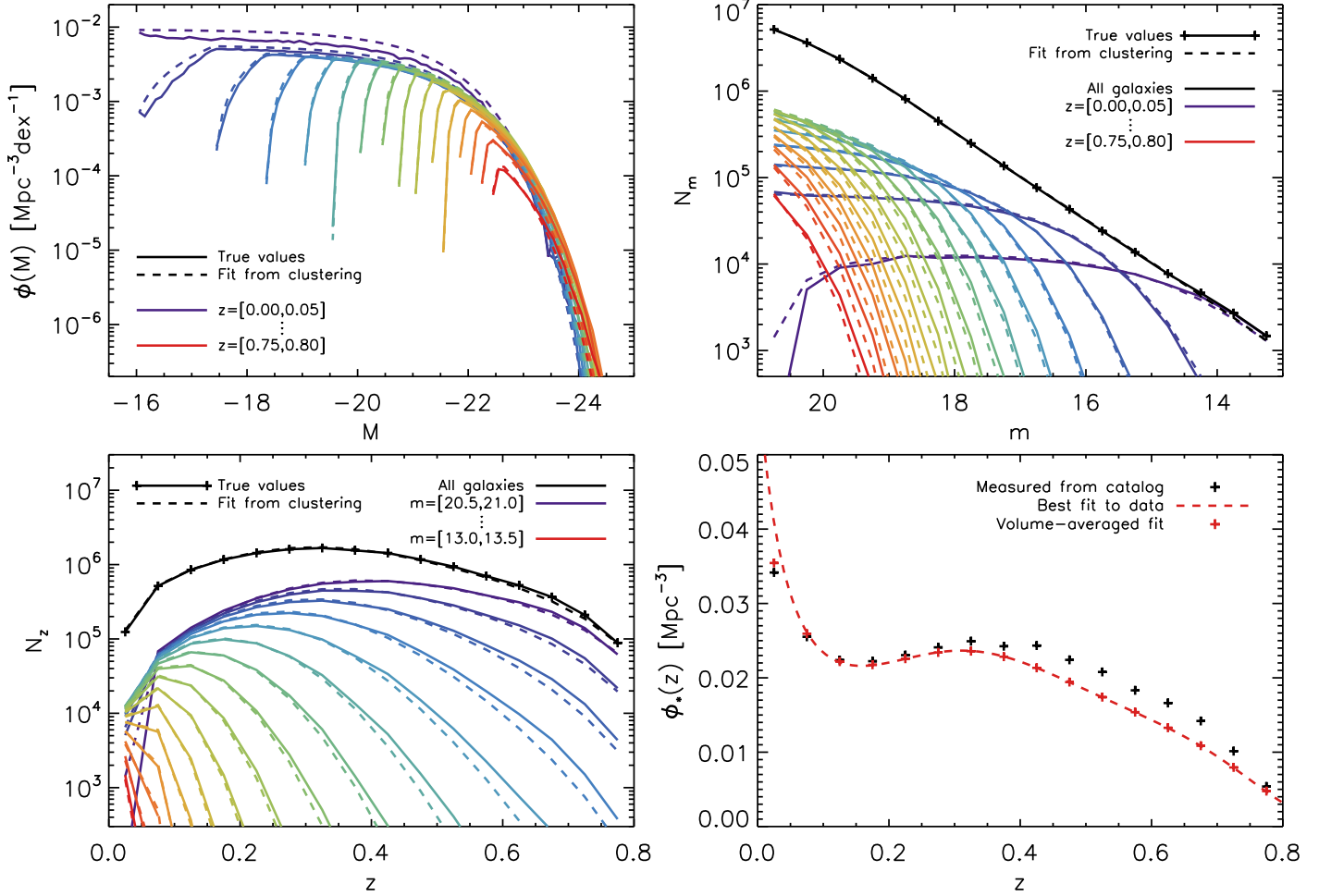


**Figure 5.** As Figure 4, but now with the Limber approximation taken. This slightly worsens the fit at high redshifts, where the clustering amplitude is small and contributions from cross-correlations between different redshift bins – which are ignored in the Limber approximation – are relatively more important. This mainly influences the luminosity function at the bright end. Still, overall the luminosity function through cosmic time is still excellently reproduced.

not necessarily mean that the luminosity function itself is not accurately reproduced, as the other panels show.

Note the sharp increase in the normalization at low redshift, which turns out to be due to the mock catalogues being centered on a large overdensity. Fortunately, the higher-order terms of the  $\phi_*$  fit are able to capture this well and reproduce the luminosity function accurately in spite of the unusually large fluctuations in galaxy number densities.

Our fiducial model has no prior information on the parameters of the luminosity function. However, it is not unreasonable to assume that the power-law slope of the luminosity function at redshift zero,  $\alpha_0$ , is well-constrained. To see how much the model outcome is influenced by the uncertainty at low redshift, we therefore also ran our model with  $\alpha_0$  fixed to the input value. The results of this test are shown in Figure 4. As expected, the panels show a marginal improvement at low redshift in comparison to the results for our fiducial model, but our results are otherwise unaffected.

Finally, we have also tested the consequences of assuming the often-used Limber approximation, by setting the clustering signal (and its covariance) to zero for the cross-correlations of spectroscopic sources in different redshift, the

results of which are shown in Figure 5. Note that we also still assume that the  $z = 0$  power-law slope  $\alpha_0$  is known. In this case, the model performs less well in regimes where the cross-correlations between different redshift bins contribute significantly – that is, at high redshift, for bright galaxies, which have relatively low number densities. Still, the overall fit is still quite good.

We present the Schechter parameters corresponding to these figures in Table 1. Note that the reproduced luminosity functions can be quite accurate even when the parameters are not, because of the degeneracies of some of these parameters with the normalization in the regime where the dim-end slope is not probed (i.e. at high redshift). This makes it all the more remarkable that the parameters obtained for our fiducial run are so close to the input parameters of the model.

When  $\alpha_0$  is held fixed, the model compensates for this by lowering  $\alpha_e$ , ensuring that the results for redshift bins beyond the first one are practically unchanged.



Run	$\alpha_0$	$M_{*0}$	$\alpha_e$	$M_{*e}$
<b>Input</b>	<b>-1.01</b>	<b>-21.5</b>	<b>-0.15</b>	<b>-0.8</b>
Fiducial	-1.076	-21.549	-0.144	-0.787
Fixed $\alpha_0$	(-1.01)	-21.501	-0.259	-0.839
+ Limber	(-1.01)	-21.478	0.027	-0.554

**Table 1.** The best-fit luminosity function parameters derived from the clustering data for each of our model runs. Parentheses indicate that the parameter was held fixed to this value.

## 4 DISCUSSION

The methods presented in this paper extend previous work by not only deriving the redshift distribution of photometric sources through clustering, but also their luminosity function through cosmic time. By testing this method on a mock galaxy survey, we have demonstrated that an input galaxy distribution over redshift and luminosity can be very accurately recovered in this way for large surveys, even when these are relatively shallow. Unlike for photometric redshifts, the redshift distributions derived are not biased by having the spectroscopic sources be selected differently from the photometric sources. As we have shown, the method returns accurate distributions and luminosity functions even if the galaxies with spectra are the brightest observed and their number densities have a vastly different redshift evolution, so long as they are in the same area of sky. Additionally, our results are not degenerate with the unknown redshift-dependent galaxy bias,  $b(z)$ .

Our goal has been to introduce a technique for measuring the luminosity function from the co-spatial combination of a deep imaging survey and a sparse spectroscopic survey and to illustrate its potential. The performance of our simple algorithm on mock data is sufficiently encouraging that further development appears warranted. In particular, application to real data would need to consider the possible effects of lensing magnification and incorporate K-corrections in the conversion between apparent and absolute magnitudes. Additionally, in this paper we have taken the following assumptions, which should be kept in mind and modified where necessary:

- First of all, we have assumed that the form of the luminosity function is known (in our case, a single Schechter function), which in real surveys may not be the case. However, one generally finds that a sum of Schechter functions is a good fit to real data. Additionally, the form of the luminosity function that one assumes in this formalism can be very versatile, and is allowed to contain many parameters to be constrained at once. We therefore do not anticipate this to be an issue in the application of the model.

- Second, we have assumed a simple luminosity bias relation (equation (7)) with a known parameter  $L'$ . We have also assumed that the redshift evolution of the remaining bias terms cancel out. However, we have imposed neither bias relation on the model, and our results imply these assumptions were sufficiently valid. There is no reason to assume, therefore, that the same would not apply to real data. Also, while the value of  $L'$  was fit to a subset of the data

prior to running the model, it could in principle be a free parameter constrained by the model.

- Third, as we mentioned in §2.3, it is difficult to define an objective value for the relative weight  $R$  of the two terms in our model's  $\chi^2$ , in equation (15). Fortunately, the outcome of the model turns out not to be very sensitive to its value. Note, however, that the ideal value of  $R$  depends on the number of redshift bins used.

We plan to test our method on DESI galaxies in a follow-up publication.

## ACKNOWLEDGEMENTS

The authors thank Joanne Cohn for helpful discussions, and Yu Feng for the use of his clustering code. This work was supported in part by the Theoretical Astrophysics Center at UCB. The Millennium Simulation databases used in this paper and the web application providing online access to them were constructed as part of the activities of the German Astrophysical Virtual Observatory.

## REFERENCES

- Benjamin J., van Waerbeke L., Ménard B., Kilbinger M., 2010, *MNRAS*, 408, 1168
- Bezanson R. et al., 2016, *ApJ*, 822, 30
- Choi A. et al., 2016, *MNRAS*, 463, 3737
- Cucciati O., Marulli F., Cimatti A., Merson A. I., Norberg P., Pozzetti L., Baugh C. M., Branchini E., 2016, *MNRAS*, 462, 1786
- Cunha C. E., Lima M., Oyaizu H., Frieman J., Lin H., 2009, *MNRAS*, 396, 2379
- Erben T. et al., 2009, *A&A*, 493, 1197
- Henriques B. M. B., White S. D. M., Thomas P. A., Angulo R., Guo Q., Lemson G., Springel V., Overzier R., 2015, *MNRAS*, 451, 2663
- Jasche J., Wandelt B. D., 2012, *MNRAS*, 425, 1042
- Kovač K. et al., 2010, *ApJ*, 708, 505
- Malavasi N., Pozzetti L., Cucciati O., Bardelli S., Cimatti A., 2016, *A&A*, 585, A116
- Matthews D. J., Newman J. A., 2010, *ApJ*, 721, 456
- McQuinn M., White M., 2013, *MNRAS*, 433, 2857
- Ménard B., Scranton R., Schmidt S., Morrison C., Jeong D., Budavari T., Rahman M., 2013, *ArXiv e-prints*
- Morrison C. B., Hildebrandt H., Schmidt S. J., Baldry I. K., Bilicki M., Choi A., Erben T., Schneider P., 2016, *ArXiv e-prints*
- Newman J. A., 2008, *ApJ*, 684, 88
- Padmanabhan N. et al., 2007, *MNRAS*, 378, 852
- Quadri R. F., Williams R. J., 2010, *ApJ*, 725, 794
- Rahman M., Mendez A. J., Ménard B., Scranton R., Schmidt S. J., Morrison C. B., Budavári T., 2016, *MNRAS*, 460, 163
- Schechter P., 1976, *ApJ*, 203, 297
- Schmidt S. J., Ménard B., Scranton R., Morrison C., McBride C. K., 2013, *MNRAS*, 431, 3307
- Schulz A. E., 2010, *ApJ*, 724, 1305
- Scottez V. et al., 2016, *MNRAS*, 462, 1683
- Sheth R. K., Rossi G., 2010, *MNRAS*, 403, 2137

**APPENDIX A: JOINT COVARIANCE MATRIX**

There are three sources of uncertainty when fitting our model to the data: uncertainties in the integrated cross-correlation function of photometric and spectroscopic galaxies,  $\bar{w}_{ps,\lambda i} \equiv \bar{w}_{ps}(m_\lambda, z_i)$ , in the integrated cross-correlation function of spectroscopic galaxies in different redshift bins,  $\bar{w}_{ss,ij} \equiv \bar{w}_{ss}(z_i, z_j)$ , and finally in the number of galaxies in the volume at some apparent magnitude and redshift,  $\tilde{N}_{p,\lambda i} \equiv \tilde{N}_p(m_\lambda, z_i)$ . For the first two, we use 2000 bootstrap resamplings to calculate full covariance matrices, while the latter is modelled as a Poisson variable with a mean given by the volume-weighted integral over the luminosity function over bins  $m_\lambda$  and  $z_i$ . Here we derive the total covariance matrix, which incorporates the uncertainties from all three sources.

To find the best-fit model, we aim to minimize  $\chi^2$  as given by equation (15), where  $C$  is the joint covariance matrix. As such,  $C$  is a  $(n_m n_z) \times (n_m n_z)$  matrix with element  $((\lambda i), (\mu j))$  given by:

$$C_{(\lambda i)(\mu j)} = \sigma(\bar{w}_{ps,\lambda i} - \tilde{w}_{ps,\lambda i}; \bar{w}_{ps,\mu j} - \tilde{w}_{ps,\mu j}) \quad (A1)$$

$$= \sigma\left(\bar{w}_{ps,\lambda i} - \sum_k X_{ik} f'_{N,\lambda k}; \bar{w}_{ps,\mu j} - \sum_l X_{jl} f'_{N,\mu l}\right),$$

where  $\sigma(A; B)$  denotes the covariance between  $A$  and  $B$ . Note that  $C$  is symmetric. As before,  $X_{ij} = \bar{w}_{ss,ij}$  and  $f'_{N,\lambda i} = K b_{L,\lambda i} \tilde{N}_{p,\lambda i} / \tilde{N}_{p,\lambda}$ , where  $K$  is a constant,  $b_{L,\lambda i}$  is the part of the bias that scales with the luminosity of a galaxy of apparent magnitude  $m_\lambda$  at redshift  $z_i$  (see equation (7)) and  $\tilde{N}_{p,\lambda} = \sum_i \tilde{N}_{p,\lambda i}$  is the total number of galaxies observed in apparent magnitude bin  $m_\lambda$ . While  $\tilde{N}_{p,\lambda}$  and  $b_{L,\lambda i}$  are known *a priori*,  $K$  is a parameter of the model. Expanding equation (A1), we find:

$$C_{(\lambda i)(\mu j)} = \sigma(\bar{w}_{ps,\lambda i}; \bar{w}_{ps,\mu j}) -$$

$$\sum_l b_{L,\mu l} \sigma\left(\bar{w}_{ps,\lambda i}; \frac{\tilde{N}_{p,\mu l}}{\tilde{N}_{p,\mu}} \bar{w}_{ss,jl}\right) -$$

$$K \sum_k b_{L,\lambda k} \sigma\left(\bar{w}_{ps,\mu j}; \frac{\tilde{N}_{p,\lambda k}}{\tilde{N}_{p,\lambda}} \bar{w}_{ss,ik}\right) + \quad (A2)$$

$$K^2 \sum_{k,l} b_{L,\lambda k} b_{L,\mu l} \sigma\left(\frac{\tilde{N}_{p,\lambda k}}{\tilde{N}_{p,\lambda}} \bar{w}_{ss,ik}; \frac{\tilde{N}_{p,\mu l}}{\tilde{N}_{p,\mu}} \bar{w}_{ss,jl}\right).$$

It is clear that  $\bar{w}_{ss,ij}$  and  $\tilde{N}_{p,\lambda k}$  should be uncorrelated, and we assume the same for  $\tilde{N}_{p,\lambda k}$  and  $\bar{w}_{ps,\mu i}$ . With this in mind, we can write:

$$\sigma\left(\bar{w}_{ps,\lambda i}; \frac{\tilde{N}_{p,\mu l}}{\tilde{N}_{p,\mu}} \bar{w}_{ss,jl}\right) = \frac{\tilde{N}_{p,\mu l}}{\tilde{N}_{p,\mu}} \sigma(\bar{w}_{ps,\lambda i}; \bar{w}_{ss,jl}), \quad (A3)$$

and:

$$\sigma\left(\frac{\tilde{N}_{p,\lambda k}}{\tilde{N}_{p,\lambda}} \bar{w}_{ss,ik}; \frac{\tilde{N}_{p,\mu l}}{\tilde{N}_{p,\lambda}} \bar{w}_{ss,jl}\right) =$$

$$\frac{\tilde{N}_{p,\lambda k} \tilde{N}_{p,\mu l}}{\tilde{N}_{p,\lambda} \tilde{N}_{p,\mu}} \sigma(\bar{w}_{ss,ik}; \bar{w}_{ss,jl}) + \quad (A4)$$

$$[\bar{w}_{ss,ik} \bar{w}_{ss,jl} + \sigma(\bar{w}_{ss,ik}; \bar{w}_{ss,jl})] \sigma\left(\frac{\tilde{N}_{p,\lambda k}}{\tilde{N}_{p,\lambda}}; \frac{\tilde{N}_{p,\mu l}}{\tilde{N}_{p,\mu}}\right).$$

All remaining covariances involving the clustering terms are

calculated directly through bootstrapping. This leaves only the last covariance in equation (A4). The  $\tilde{N}_{p,\lambda i}$  are mutually independent Poisson variables, but are not independent of  $\tilde{N}_{p,\mu}$  when  $\mu = \lambda$ . So:

$$C_{(\lambda i)(\mu j)} = \sigma(\bar{w}_{ps,\lambda i}; \bar{w}_{ps,\mu j}) -$$

$$\sum_k f'_{N,\lambda k} \sigma(\bar{w}_{ps,\mu j}; \bar{w}_{ss,ik}) -$$

$$\sum_l f'_{N,\mu l} \sigma(\bar{w}_{ps,\lambda i}; \bar{w}_{ss,jl}) + \quad (A5)$$

$$\sum_{k,l} f'_{N,\lambda k} f'_{N,\mu l} \sigma(\bar{w}_{ss,ik}; \bar{w}_{ss,jl}) +$$

$$\delta_{\lambda\mu} \sum_{k,l} K^2 b_{L,\lambda k} b_{L,\mu l} [\bar{w}_{ss,ik} \bar{w}_{ss,jl} +$$

$$\sigma(\bar{w}_{ss,ik}; \bar{w}_{ss,jl})] \sigma\left(\frac{\tilde{N}_{p,\lambda k}}{\tilde{N}_{p,\lambda}}; \frac{\tilde{N}_{p,\mu l}}{\tilde{N}_{p,\lambda}}\right).$$

Since  $\tilde{N}_{p,\lambda}$  is a sum of independent Poisson variables, and therefore a Poisson distributed variable itself, we need to know the covariance between ratios of dependent Poisson variables in the domain  $[0, 1]$ . Analytical expressions for this (co)variance and its derivatives can be derived, and the former are given below for completeness. Here  $\gamma$  is Euler's constant, and Ei is the exponential integral function.

If  $k = l$ :

$$\sigma^2\left(\frac{\tilde{N}_{p,\lambda k}}{\tilde{N}_{p,\lambda}}\right) = \frac{\tilde{N}_{p,\lambda k}}{\tilde{N}_{p,\lambda}^2} e^{-\tilde{N}_{p,\lambda}} \left\{ \tilde{N}_{p,\lambda k} (1 - e^{-\tilde{N}_{p,\lambda}}) + \right. \quad (A6)$$

$$\left. (\tilde{N}_{p,\lambda} - \tilde{N}_{p,\lambda k}) (\text{Ei}[\tilde{N}_{p,\lambda}] - \gamma - \ln[\tilde{N}_{p,\lambda}]) \right\}.$$

In all other cases:

$$\sigma\left(\frac{\tilde{N}_{p,\lambda k}}{\tilde{N}_{p,\lambda}}; \frac{\tilde{N}_{p,\mu l}}{\tilde{N}_{p,\lambda}}\right) = \frac{\tilde{N}_{p,\lambda k} \tilde{N}_{p,\mu l}}{\tilde{N}_{p,\lambda}^2} e^{-\tilde{N}_{p,\lambda}} (1 - e^{-\tilde{N}_{p,\lambda}} -$$

$$\text{Ei}[\tilde{N}_{p,\lambda}] + \gamma + \ln[\tilde{N}_{p,\lambda}]). \quad (A7)$$

This paper has been typeset from a  $\text{\LaTeX}$  file prepared by the author.